

Global projections of compound coastal meteorological extremes

Emanuele Bevacqua^{*1,2}, Michalis I. Vourdoukas³, Giuseppe Zappa^{1,4}, Kevin Hodges¹,
Theodore G. Shepherd¹, Douglas Maraun², Lorenzo Mentaschi³, and Luc Feyen³

April 13, 2020

1. Department of Meteorology, University of Reading, Reading, United Kingdom.
2. Wegener Center for Climate and Global Change, University of Graz, Graz, Austria.
3. European Commission, Joint Research Centre (JRC), Ispra, Italy.
4. Istituto di Scienze dell'Atmosfera e del Clima, ISAC-CNR, Bologna 40129, Italy.

*e-mail: e.bevacqua@reading.ac.uk

Keywords. Meteorological extremes, compound flooding, future projections, anthropogenic climate change, coastal hazard, cyclones, dependence, copulas.

Compound coastal and inland flooding can result in catastrophic impacts in densely populated low-lying coastal areas. The dynamics and interactions between the underlying meteorological drivers in view of climate change are not fully understood at global scale. Here, we show that under a high emissions scenario the concurrence probability of extreme meteorological tides and inland precipitation would increase by more than 30% on average along coastlines worldwide by 2100 compared to present. In latitudes above 40° north, compound meteorological extremes would become more than 2.5 times as frequent, while they would happen less frequently in parts of the subtropics. Climate-induced dynamics in precipitation extremes contribute to about 80% of the projected change in concurrence probability, while dynamics in meteorological tides account for 16% and those in the dependence between the two extremes for 4%. Our results indicate that not accounting for these effects in adaptation planning could leave coastal communities insufficiently protected against flooding.

Introduction

A considerable portion of the global population lives in low-lying coastal areas that are at risk of flooding from sea-level^{1,2,3} and precipitation/river discharge extremes^{4,5,6,7}. The concurrence or short succession of these two hazards can cause compound flooding that can result in larger impacts than those caused by the individual hazards^{8,9,10}, as exemplified by recent high-impact events like hurricanes Harvey, Irma, and Maria^{11,12}. Compound flooding occurs when inland rainfall flood potential is enhanced by high meteorological tides that obstruct the gravity-driven drainage of excess fluvial and/or pluvial water into the sea^{13,14}, or when flooding from meteorological

tides is amplified by precipitation⁸.

Compound flooding has been studied at local to global scale for present climate. Studies of recent mid-latitude events have increased the understanding of the mechanisms driving compound flooding^{14,15,16,17,18,19}. At a larger scale, present-day compound flood hazard has been assessed for the US⁸, Australia^{20,21}, and Europe^{9,10,13,22,23,24} considering co-occurring sea-level and precipitation (or river discharge) extremes. Most of these large-scale studies used field observations that do not cover the entire global coastline^{10,12}. Recent advances in ocean modelling has resulted in the generation of sub-daily continuous time-series of sea levels with global coverage^{1,25} that enable comprehensive global assessments of present-day compound flood hazard^{26,27}.

Sea level rise (SLR) will push mean and extreme sea levels upward¹. A study by Moftakhari et al.²⁸ at eight estuarine systems along the coasts of the United States shows that this will increase compound flood hazard in the future. However, ultimately flooding in coastal zones is driven by extreme meteorological conditions. Hence, combined and interrelated effects of changes in intense precipitation^{5,29} and meteorological tide¹ in view of global warming can alter compound flood hazard in low-lying coastal areas around the world. These effects were not considered in Moftakhari et al.²⁸ and have only been studied for Europe¹⁰, while a global overview is missing.

Here we present a first comprehensive global analysis of compound meteorological extremes in present and future climate. We combined outputs from global climate models (GCMs) and ocean models in order to assess the spatio-temporal dynamics of the meteorological drivers of compound flooding along the global coastline during this century. Daily time series of storm surges¹ and waves^{1,30,31} were available from ocean model simulations forced with reanalysis data for the present³² and with CMIP5 GCM climate projections up to the end of the century under a high emissions scenario (RCP8.5)³³. Daily precipitation time series from the reanalysis data and GCMs in the neighbouring coastal zone were aggregated over 3-day windows^{8,10,27,34}. We define extremes of meteorological tide and precipitation as events that occur on average once a year in the present climate and assessed the joint return period of concurring extremes in present and future climate³⁵. Concurrence probabilities (or inversely return periods) were computed from the bivariate distribution of meteorological tides and precipitation based on parametric copulas that model the pairs of high values only^{8,10}.

Results

Present-day concurrence of extreme precipitation and meteorological tide

Present-day concurrence probabilities of ocean and inland meteorological extremes, expressed as joint return period, are mapped in Figure 1 and summarised per IPCC region in Supplementary Table 1. Low joint return period values indicate higher dependency between extremes in precipitation and meteorological tide, with a value of 365 years expected under complete independence. The global median return period of 18 years shows that in the majority of coastlines around the world, ocean and inland meteorological extremes are strongly correlated and roughly 20 times more likely to co-occur compared to when they would be independent. There is, however, strong spatial variability in concurrence probability, with joint return periods that can vary several orders in magnitude.

Cyclonic configurations cause strong surface winds and low atmospheric pressure at the sea surface with consequent high meteorological tides^{10,17}. As a result, concurrent extreme precipitation and high meteorological tides are primarily driven by low-pressure systems (Supplementary Fig. S1)^{8,10}. The highest concurrence probability (lowest joint return period) at present is therefore observed in regions with high tropical (TC) or extratropical (ETC) cyclone activity, such as the US, eastern Central America, eastern Madagascar, Europe, northern Africa, northern and eastern Australia, India, northern Southeast Asia, China, and Japan (Fig. 1 and Fig. 2a,b). In these

regions, extreme precipitation and meteorological tides presently coincide every 4 to 8 years. Off the west coast of Central America and Mexico, TCs are also frequent but they usually do not cross the coast (Fig. 2b), which results in somewhat higher joint return periods (8-16 years). Overall, extensive tropical regions with low cyclonic activity exhibit low concurrence probabilities (Fig. 1 and Fig. 2a,b). While cyclones cause high sea water levels, high cyclonic activity not necessarily implies a high probability of concurrent intense precipitation. For example, although cyclones are more frequent over northern Europe than the Mediterranean Sea (Fig. 2a), the two regions show comparable joint return periods (Fig. 1) because the fraction of precipitation extremes caused by cyclones is similar among the two regions³⁶. In addition, even with high cyclonic activity and the relevance of cyclones for precipitation extremes the regional concurrence probability can be low. This is particularly the case when high meteorological tides and precipitation extremes are caused by different cyclone types (e.g. cyclones tracking on different pathways)²², e.g. in the northern Baltic Sea, western Japan, and western Sardinia (Italy) (Supplementary Fig. S2). We find in general that in areas with a low concurrence probability, coastal and inland meteorological extremes tend to happen in different seasons (see similar spatial distribution of blue areas in Fig. 1 and Supplementary Fig. S3a).

The highest number of concurring meteorological ocean and inland extremes in the tropics tend to occur in the TC season (Fig. 2c). This is during May-November in central America, October-May around Madagascar and northern Australia, April-December around India, and April-January in the Typhoon region. Similarly, at midlatitudes the concurrence frequency peaks around autumn-winter, when the ETC activity is highest³⁶. The longest season with concurrent extreme events is found along the eastern US coast (Fig. 2d), where they are caused by both TCs and ETCs⁸ that hit the coast in different seasons. Our findings on present-day dependency between the meteorological drivers of compound flooding agree in general with those observed in previous regional and global scale studies (see discussion in SI).

Projections of concurrent extremes in precipitation and meteorological tide

Under a high emissions scenario (RCP8.5), the meteorological drivers of compound flooding are projected to co-occur more frequently along 62% of the global coastline by the end of this century (Fig. 3a). The global median change in return period ΔT is -24% , which corresponds to joint extreme events becoming 32% more probable. The concurrence probability is projected to increase the most in the Northern Hemisphere at latitudes above 40° north (see red line in Fig. 3b), with the frequency of joint events by 2100 projected to be on average 2.6 times higher compared to present (median $\Delta T = -62\%$). The rise in frequency is particularly evident for coasts in northern North America, northern Europe, northern Mediterranean, Russia, Japan, the Korean peninsula, China, Bangladesh, and around Cameroon (Fig. 3a). Similar trends are also projected in parts of the Southern Hemisphere, such as for coastlines in northwestern South America, southern Chile, northern Australia, the Gulf of Carpentaria and New Zealand. Concurrent events are projected to become significantly less probable along a smaller portion of the global coastline (see blue line in Fig. 3b), most notably in northwestern Africa, southern Spain, western South Africa, eastern Madagascar, southwestern Australia, and Central Chile. Results are more uncertain in several areas of the tropics and subtropics (magenta line in Fig. 3b), such as in the Caribbean and in Southeastern Asia (see magenta points in Fig. 3a).

Present-day return period of concurrent extremes

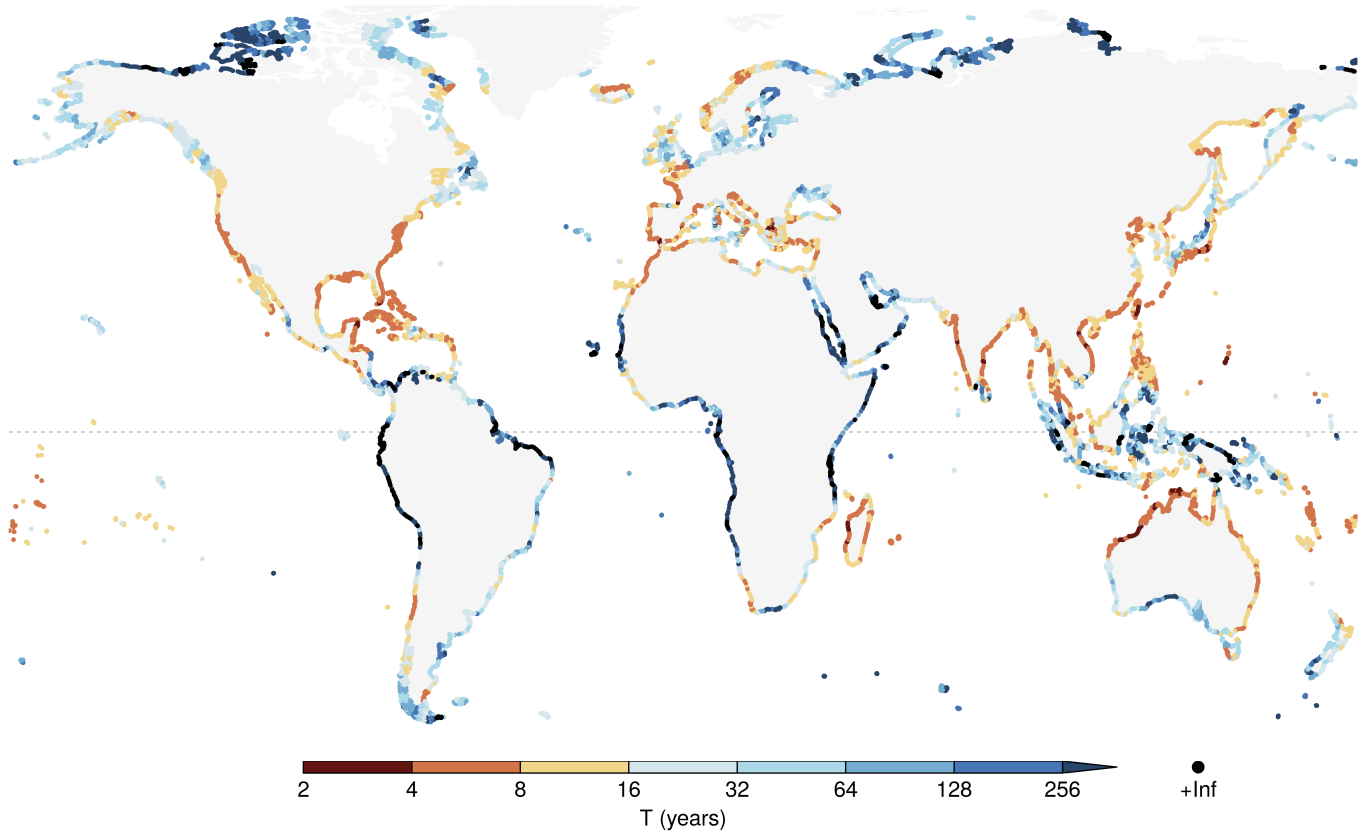


Figure 1: **Present-day return period of concurrent extremes in precipitation and meteorological tide.** Return period (inversely probability) of co-occurring extremes based on the ERA-Interim data (1980-2014).

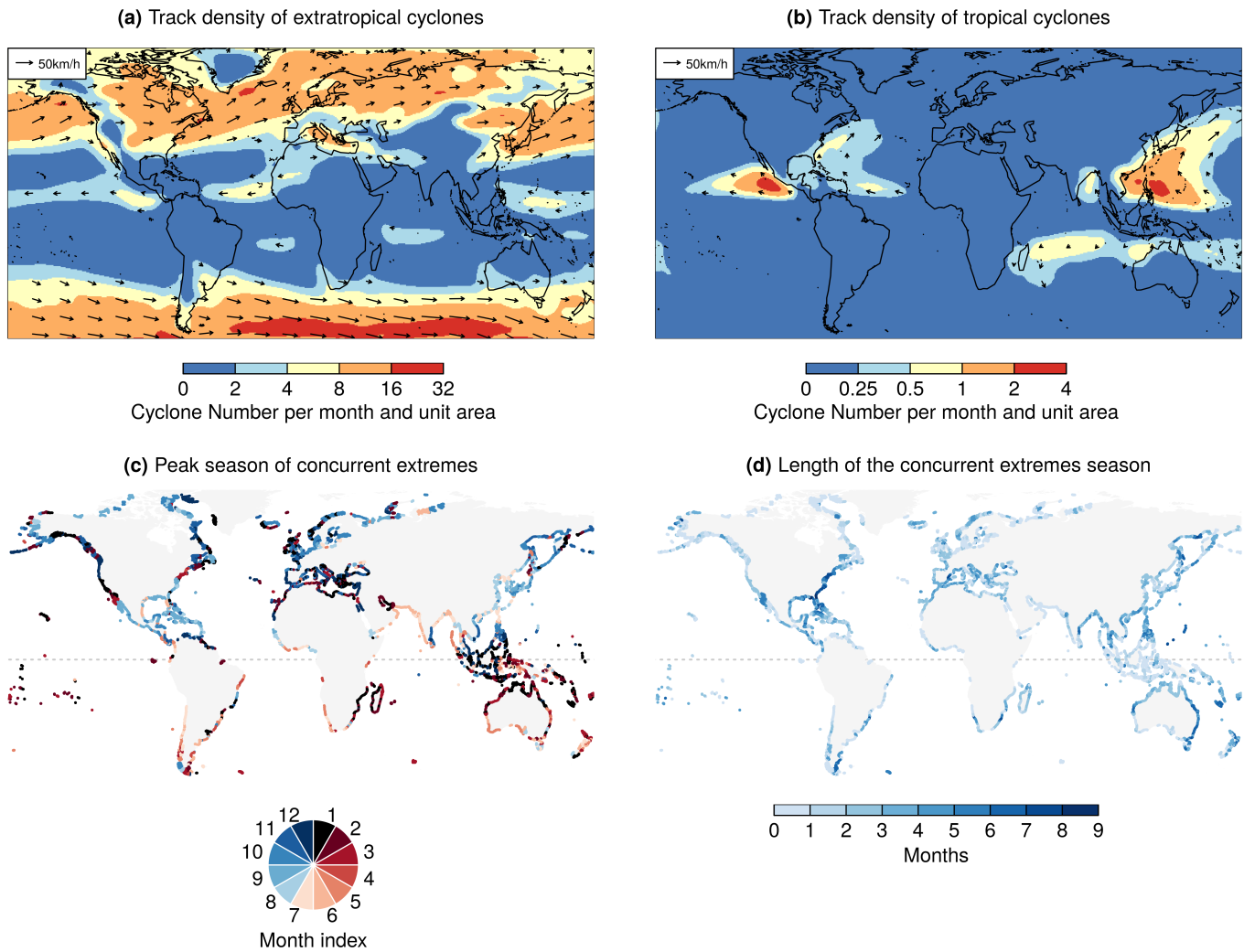


Figure 2: **Drivers and seasonality of present-day concurrent extremes in precipitation and meteorological tide.** Track density of (a) extratropical cyclones from ERA-Interim and (b) tropical cyclones from IBTrACS³⁷. Values express the number of cyclones per month per unit area (equivalent to a 5° spherical cap). Arrows show the mean translation speed of cyclones. (c) The month with the highest concurrence of extremes and (d) length of the concurrence season, based on ERA-Interim. The length of the concurrence season was defined as the shortest possible period where 90% (range defined by the 5-95th percentiles) of concurrent extremes were observed. Extremes are defined based on the 99.5th percentiles.

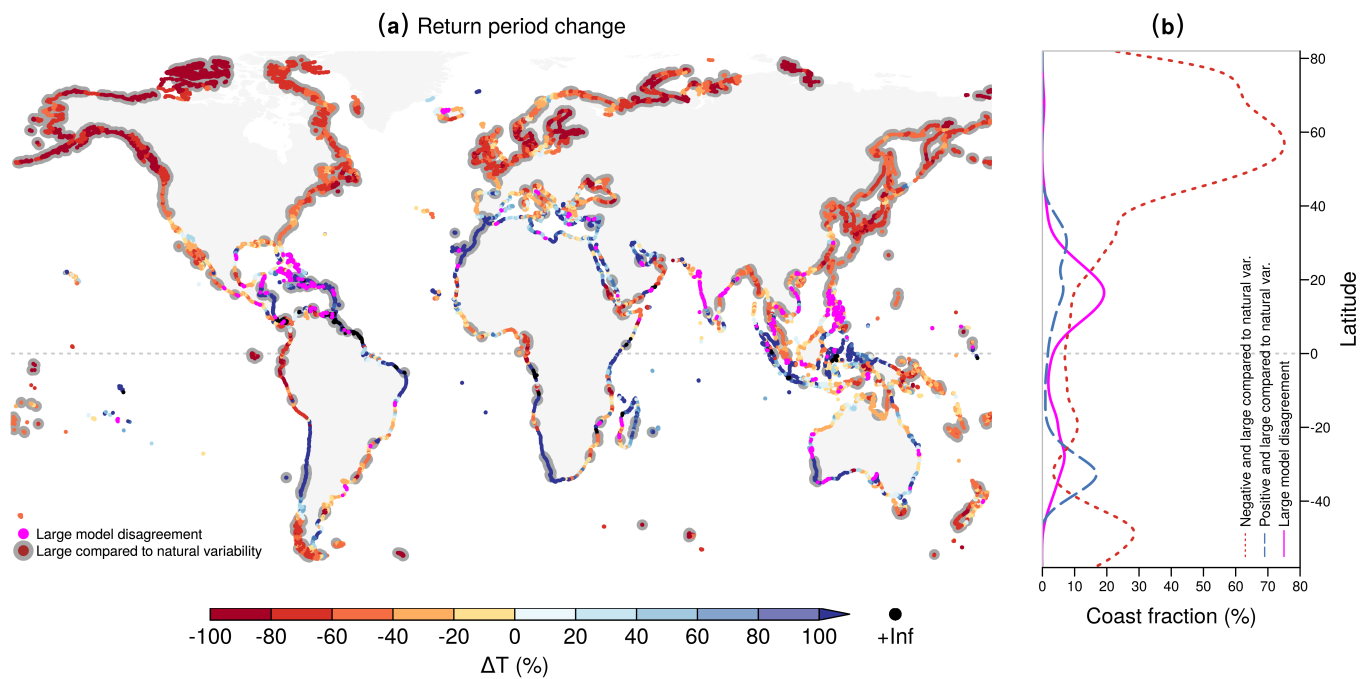


Figure 3: **Future changes in the return periods of concurrent meteorological drivers of compound flooding.** (a) Ensemble median projected change (%) of joint return period (inversely probability) between future (2070-2099) and baseline (1970-2004) climate. Dots with a grey background indicate locations where the projected change is robust, i.e. the ensemble median change lies outside the present-day 95% confidence interval and at least five out of six models agree on the sign of the change. Magenta indicates locations with high model disagreement, i.e. where at least two models project large (lying outside the present-day 95% confidence interval) positive trends and at least two models project large negative trends. (b) Coastline fraction per 5° of latitude (smoothing spline) with a robust negative change (red dotted line), robust positive change (blue dashed line), and high model disagreement (magenta solid line).

Drivers of changes in concurrent meteorological extremes in coastal areas

Changes in precipitation extremes are the key driver of the projected changes in compound meteorological extremes (Fig. 4a,b; global median $\Delta T_{\text{prec.}} = -26\%$), increasing the concurrence frequency for 84% of coasts worldwide. Aggregated at global level, the relative contribution is 80% (Supplementary Table 1). Changes in meteorological tides have a weaker effect (Fig. 4c,d; global median $\Delta T_{\text{met. tide}} = +5\%$). While they reduce the probability of concurrent extremes along 59% of the global coastline, their global relative contribution to the projected changes in concurrence frequency is 16% (Supplementary Table 1). The effects of changes in the dependence between high meteorological tides and extreme precipitation can be locally pronounced for single climate realisations but the average effects over the ensemble of climate projections are generally small compared to natural variability (Fig. 4e,f). Changes in the dependence structure do not exhibit a clear large-scale spatial pattern and compensate each other at the global scale ($\Delta T_{\text{dep.}} = -1\%$), with approximately balanced fractions of coast with either increasing or decreasing dependency. As a consequence, they increase concurrence probability in 51% of the global coastline, while reducing it in 49%, resulting in a global overall contribution of 4% (Supplementary Table 1).

At the regional level, changes in precipitation are the main driver in all IPCC regions apart from South Europe and South Africa where changes in meteorological tides dominate, and the Amazon, North Australia, North East Brazil, Sahara, and West Asia where changes in the dependence dominate the signal (Supplementary Table 1). The dynamics in extreme precipitation increase the probability of concurrent events everywhere apart from the Sahara region. On the contrary, projected changes in meteorological tides decrease concurrence frequency everywhere but in Alaska/NW Canada, Central Europe, East Canada, East and West Africa, East Asia, North Europe, South East and West North America.

Precipitation extremes are expected to intensify and happen more frequently in most coastal areas worldwide due to the thermodynamic increase in atmospheric moisture content⁵, and consequently the likelihood to have joint inland and coastal meteorological extremes. However, changes in atmospheric circulation can further modulate and potentially oppose this thermodynamic effect. This is the case along the coasts of northern and southwestern Africa, Central Chile, and southwestern Australia, where a more stable atmosphere leads to weaker vertical motions. This, in turn, reduces the intensity of precipitation extremes⁵ and consequently the probability for concurrent events in these confined areas (Fig. 4a).

Although the effect of changes in meteorological tide on the projected joint occurrence probability is in general small compared to the natural variability (see Fig. 4d and rare grey dots in Fig. 4c), the spatial patterns are consistent with the projected anthropogenic-driven changes in cyclone activity^{38,39,40}. For example, in Europe, our projections of concurrence frequency are mostly in agreement with the projected decrease in winter storm frequency and intensity in the Mediterranean Sea³⁹ and the increase in storm track activity in northern Europe^{38,39}. This results in a respective decrease and increase in meteorological tides in these two regions¹ and the consequent changes in the concurrence probability. In the Baltic Sea this effect of the increase in meteorological tides is most notable and robust compared to natural variability (grey dots in Fig. 4c). The projected increase in joint occurrence probability for western Canada (Fig. 4c) is consistent with a poleward shift in the north Pacific boreal winter jet stream and in the associated storm-track^{38,40,41}. A similar storm track poleward shift⁴⁰ appears consistent with the projected changes in joint return period for New Zealand, southern Australia, and southern South America (Fig. 4c). Lower meteorological tides projected in parts of the equatorial region lead to a reduction in the concurrence probability, especially in Asia (Fig. 4c,d).

Atmospheric circulation dynamics can affect meteorological tide and precipitation extremes in a similar manner, for example, through a weakening (or strengthening) of the regional cyclone activity. As a result, meteorological tide- and precipitation-related changes in the concurrence probability qualitatively demonstrate a positive relation, which is modulated by an offset due to the spatially-homogeneous

thermodynamic-driven enhancement of precipitation extremes⁵ (Supplementary Fig. S4). For example, reduced cyclonic activity causes a reduction in meteorological tide and precipitation extremes, and therefore in concurrence probability, in northwestern and southern Africa, Central America, Central Chile, and along a large part of Australia's coastlines (compare Fig. 4a and 4c; see also Fig. 4b from Pfahl et al.⁵). On the contrary, a concurrent increase in meteorological tide and precipitation extremes results in more frequent compound extremes, e.g. in northern Europe, western Canada, and Alaska. The thermodynamic-driven offset is visible, e.g., in the Mediterranean Sea where a weakened cyclonic activity³⁹ reduces meteorological tides (Fig.4c) and negatively modulates precipitation⁵, but a moistened atmosphere cause more intense precipitation extremes⁵ (Fig.4a; Supplementary Table 1).

Uncertainty in projections

The uncertainty in the projections of future concurrence probability is dominated by the uncertainty in the dependence between meteorological extremes. At the global scale, climate variability in the projected dependence accounts for approximately half of the uncertainty in the projections of compound meteorological extremes. Precipitation and meteorological tide related uncertainty in the projections are comparable and account for the other half (Fig. 5). Also at the level of IPCC regions, uncertainty in the dependence is the main driver of the future concurrence uncertainty. In certain regions, pronounced but contradicting projections of changes in the dependency (magenta points in Fig. 4e) result in a high uncertainty in the overall response of the concurrence probabilities (magenta points in Fig. 3a), especially in central America that is often hit by TCs. Wahl et al.⁸ found that without trends in the records of the individual meteorological drivers, compound events have already increased along some parts of the US coastline due to a shift towards storm surge weather patterns that also favour high precipitation. The large variability in our projections of the dependence dynamics indicate that there is large uncertainty on how climate change could alter the concurrence of meteorological extremes in addition to the effects of changes in the marginal drivers. The findings also indicate that considering the variability of the dependence is crucial to avoid overconfident and potentially misleading projections of the future risk.

Uncertainty in the projections of precipitation and meteorological tide extremes is also relevant. Thermodynamic driven changes in precipitation extremes are a robust feature of climate models. There is, however, less confidence in the magnitude of climate-induced atmospheric circulation changes⁴², which exerts a strong control on meteorological tides and regionally modulates precipitation extremes. Hence, despite the consistency among climate models in the sign of the projected changes in precipitation extremes, the magnitude of the changes is uncertain, especially in the tropics⁵. At midlatitudes, also projections of wind extremes that modulate meteorological tides show large climate variability because of uncertainty in the evolution of atmospheric circulations⁴¹.

Discussion

This study provides the first global assessment of the possible effects of climate change on the meteorological drivers of compound flooding. Our estimates should not be interpreted as actual compound flood hazard^{10,12,26,43}. Rather, we studied the probability of co-occurrence of extremes in meteorological tide and precipitation in coastal areas. When these extremes co-occur, actual flooding will depend on a variety of additional factors. Coastal flooding usually happens during high tides^{10,44} that do not depend on meteorological conditions. In addition, actual flooding only takes place when flood protection or natural barriers are overtopped or breach and low-lying lands become inundated. Here, we analysed the potential for local rainfall-driven compound flooding. Similar spatial patterns between

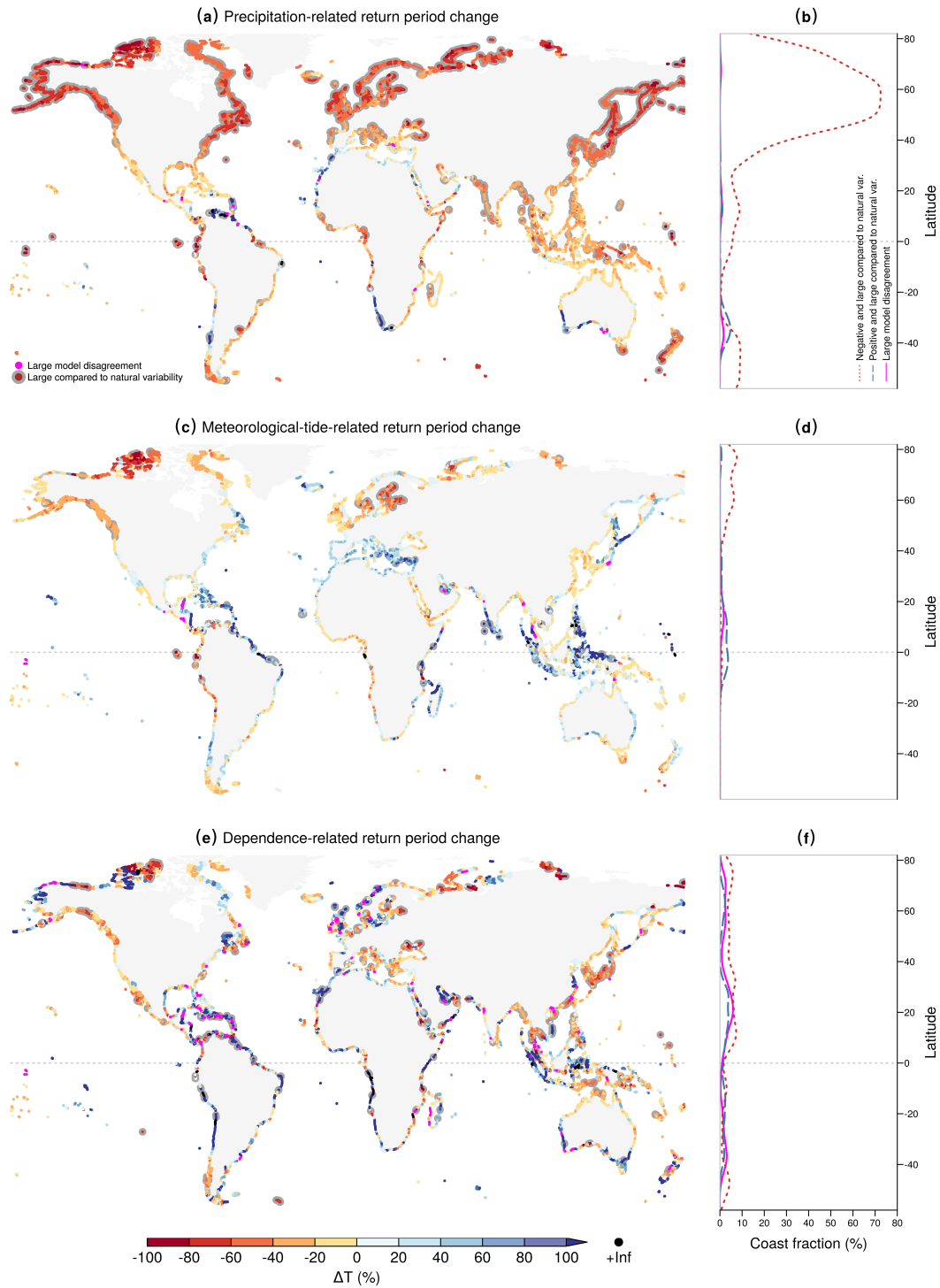


Figure 4: **Attribution of projected changes in joint return periods to changes in precipitation, meteorological tides, and their dependence.** (a) Ensemble median projected change (%) of joint return periods (inversely probability) between future (2070-2099) and baseline (1970-2004) when only taking into account the projected changes in precipitation ($\Delta T_{\text{prec.}}$). (b) Coastline fraction per 5° of latitude (smoothing spline) with a robust negative change (red dotted line), robust positive change (blue dashed line), and high model disagreement (magenta solid line). (c-f) Similar results as (a-b), but for joint return period changes when only taking into account the projected changes in the meteorological tide ($\Delta T_{\text{met. tide}}$) (c-d), and in the dependence between meteorological tide and precipitation ($\Delta T_{\text{dep.}}$) (e-f).

Relative contributions to uncertainty in return period changes

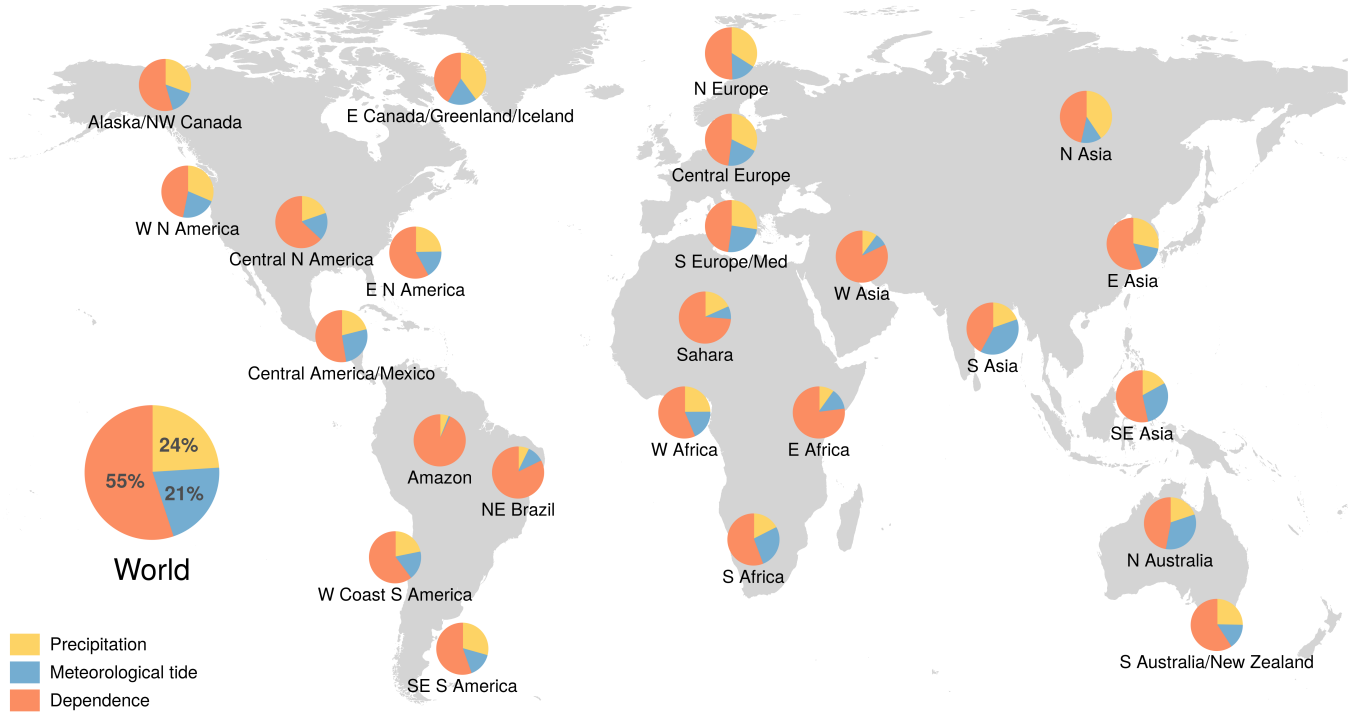


Figure 5: Drivers of uncertainty in the projected changes of the joint return period of concurrent precipitation and meteorological tide extremes for IPCC subregions and worldwide. Relative model uncertainty in the projected change in joint return periods (inversely probability) between the future (2070-2099) and baseline (1970-2004) climates driven by the individual meteorological drivers of compound flooding, i.e. only by precipitation, meteorological-tide, and their dependence (see Methods). The IPCC subregions are shown in Supplementary Fig. S6.

precipitation and riverine compound flood potential were found by Bevacqua et al.²⁷. However, considering precipitation only close to sea not necessarily represents well compound flood hazard in estuaries of long rivers (catchment $\gtrsim 5\text{-}10,000\text{ Km}^2$)²⁷, for which high discharges close to the coast are influenced by several processes over the catchment inland^{12,27}.

By the end of this century, SLR could push up mean sea levels and meteorological tides by one meter or more¹. This upward shift will strongly increase the probability to experience what is today an extreme meteorological tide and consequently of compound flooding if coastal protection is not adjusted for SLR. Moftakhari et al.²⁸ projected how SLR will increase the probability of compound flooding for a number of estuaries in the United States through this mechanism. We show that also changes in the joint probability of having high meteorological tides (on top of the elevated mean sea level) and extreme precipitation could considerably affect compound flooding, a process not considered by Moftakhari et al.²⁸. Our projections vary strongly between regions, but globally averaged the triggering conditions of compound flooding are projected to become one third more probable under a high emissions scenario by 2100. At latitudes above 40° north this would happen more than 2.5 times as frequent compared to the present. Despite limitations inherent to a global scale analysis^{10,25,26,45,46} (see extensive discussion in a dedicated section in the Methods), our study provides insight into large-scale the spatio-temporal dynamics of compound flood drivers in view of climate change. Local assessments focussing on hotspot regions with robust changes could provide more accurate assessments of compound flood hazard and its impacts^{14,16,17,47}.

Coasts will be particularly exposed to the effects of global warming through a range of climate change processes⁴⁸. Adaptation targeted at protecting coastal communities should not only take into account expected SLR^{2,49} or projections of total extreme sea levels⁵⁰, but also dependencies with inland meteorological extremes. Neglecting compound flood hazard and changes therein might leave several parts of the global coastline insufficiently protected. The increase in frequency of concurrent events could make adaptive measures more complex and expensive, but also pose a challenge for emergency response procedures that would need to cope with more frequent, simultaneous natural hazards^{11,51}.

Acknowledgements. EB and GZ acknowledge financial support from the European Research Council grant ACRC (project 339390). EB acknowledges support from the Volkswagen Foundation's (CE:LLO project, grant no. 88468). EB and DM acknowledge the European COST Action DAMOCLES (CA17109).

Competing interests. The authors declare no competing interests.

Methods

Data. Meteorological tides were obtained from Vousdoukas et al.¹. Waves were simulated with Wavewatch III^{1,30,52} (forced with 6-hourly wind field). Storm surges were modelled with D-FLOW Flexible Mesh (FM) using a flexible mesh setup (forced by 6-hourly wind and atmospheric pressure fields)^{1,25,52,53}. The resulting sea level data are available every ~ 100 km along the global coastline. Precipitation was taken from the climate model grid point nearest to each coastal location. Detailed information on the sea-level dataset and models can be found in the references^{1,10,25,30,52,53}, including data validation. Sea level and precipitation data are based on ERA-Interim³² (period 1980-2014) and six CMIP5 models³³ (periods 1970-2004 and 2070-2099) (i.e., ACCESS1-0, ACCESS1-3, GFDL-ESM2M, GFDL-ESM2G, CSIRO-Mk3-6-0, and EC-EARTH). The GFDL-ESM2G model is not considered for the Black Sea and the Red Sea coasts because of instabilities of the surge model. Tropical cyclones (TCs) are unsatisfactorily resolved by the coarse

resolution of CMIP5 models⁵⁴. We therefore improved the representation of TC-driven meteorological tides (storm surges and waves) in the reanalysis based dataset. Storm surges caused by TCs were forced by dynamically downscaled atmospheric conditions and waves were corrected for TC effects based on satellite altimetry data (see Vousdoukas et al.¹ for more details). For information on models' skill in representing joint return periods of concurrent extreme precipitation and meteorological tide, see Supplementary Fig. S5.

Discussion about the modelling limitations. The results should be interpreted considering some inevitable limitations, which are common in large-scale studies. We use global climate simulations of future meteorological drivers and it is well known that higher-resolution input data could improve the representation of both meteorological tide^{1,25} and precipitation extremes⁵⁵. The effect of resolution is even stronger regarding the representation of TCs^{25,46,54}. Despite the effort here to improve the representation of tropical cyclones and overall satisfactory representation of the joint return periods in the present climate (Supplementary Fig. S5), the projected changes in regions subject to high TC activity should be interpreted with caution. The same applies to the findings at high latitudes, where precipitation often occurs as snow and waves/currents interacting with sea ice are currently not considered in the modelling. Similarly, physical interactions between waves, storm surges, astronomical tides, SLR, precipitation, and hydrology are not resolved^{56,57,58,59}. Therefore it is assumed that sea water level components are independent. This is inevitable for a global analysis given the current modelling capacity. However, studies have demonstrated that assuming no interaction between the sea level components is acceptable given the overall uncertainty in the climate change projections^{1,60,61,62}. Overall, we are confident that the above limitations do not distort our findings and that our study expands the understanding of present and future global compound flooding hazard. This is supported by the fact that our findings are physically consistent with studies of large-scale atmospheric circulation changes employing larger model ensembles than the present one^{5,38,39,40,41,63,64}.

Cyclone tracking. Extratropical cyclone (ETC) tracks were identified based on the objective feature tracking algorithm TRACK^{65,66}. Following Hoskins and Hodges (2002)⁶⁷, the algorithm uses the 850hPa relative vorticity to identify and track cyclones in both hemispheres. Tropical cyclone tracks were obtained from the observation-based IBTrACS dataset³⁷. For both the tropical and ETC datasets, the spatial maps of cyclone track density were computed using spherical kernel density estimators⁶⁸.

Return periods. We assessed the bivariate return periods⁶⁹ of concurring heavy precipitation and high sea-level (individual 99.7th percentiles). The bivariate return period that we used - so-called "AND"^{35,70,71} - allows for disentangling flooding caused by the concurrence of high sea-level and precipitation values. To estimate return periods, we applied a parametric copula-based bivariate probability distribution to pairs of meteorological component of sea-level and precipitation that are simultaneously high, i.e., that exceed the individual 95th percentiles (s_{sel} and p_{sel} , respectively). In locations where few pairs were selected we reduced the selection threshold to below 0.95 in order to ensure that at least 20 pairs of values were selected. We replaced groups of selected event pairs separated by less than 3 days by a unique event having the maximum precipitation P and meteorological component of sea-level S observed in the group. We define the bivariate return period as:

$$\begin{aligned}
 T(s_{99.7}, p_{99.7}) &= \frac{\mu}{P((s > s_{99.7} \text{ and } p > p_{99.7}) | (s > s_{sel} \text{ and } p > p_{sel}))} = \\
 &= \frac{\mu}{1 - u_{S99.7} - u_{P99.7} + C_{SP}(u_{S99.7}, u_{P99.7})}
 \end{aligned}
 \tag{1}$$

where μ is the average time elapsing between the selected pairs, $u_{p99.7} = F_P(p_{99.7})$, F_P is the marginal cumulative distribution of the excesses over the selection threshold of the precipitation variable (accordingly for sea level), and C_{SP} is the copula modelling the dependence between the selected pairs. We fitted copulas from the families Gaussian, t, Clayton, Gumbel, Frank, Joe, BB1, BB6, BB7, BB8 to (u_S, u_P) (obtained via empirical marginal cumulative distribution function (CDF)⁷¹), and then we selected the best-ranked family according to Akaike information criterion. We modelled the marginal distributions of precipitation and sea level beyond the selection thresholds by a Generalised Pareto Distribution. Copulas and marginal distributions were fitted through a maximum likelihood estimator (using the *VineCopula*⁷² and *ismev*⁷³ R-packages). The goodness of fit of copulas and marginals was tested via the Cramer-von-Mises criterion (via the *VineCopula*⁷² and *eva*⁷⁴ R-packages, respectively).

Return periods changes and robust changes. For the individual CMIP5 models, the changes (%) in the return periods (e.g., in Fig. 3a) were estimated as $\Delta T(\%) = 100 \cdot (T^{2070-2099} - T^{1970-2004}) / T^{1970-2004}$. Based on physical interpretation, when both $T^{2070-2099}$ and $T^{1970-2004}$ are infinite, $\Delta T(\%)$ is set to 0%; when $T^{2070-2099}$ is finite and $T^{1970-2004}$ is infinite, $\Delta T(\%)$ is set to -100%. A *robust* (large compared to natural variability) return period change is defined as the case where the multi-model median of the return period change lies outside the present-day 95% range due to natural variability (estimated with a resampling approach⁸, see the next section) and at least five out of six models agree on the sign of the change.

Given the inverse relationship between return period and probability³⁵, it can be estimated that $\Delta P(\%) = -100 \cdot \Delta T(\%) / (\Delta T(\%) + 100)$, where the percentage change in probability is defined similarly to the change in return period.

Present-day range of the return period due to natural variability. The present-day range in the return period due to natural variability was estimated (for ERA-Interim) as a 95% confidence interval based on resampling the interannual variability. For each location, we randomly sampled $N_{\text{bootstrap}} = 700$ bivariate time series of precipitation and meteorological tides, and computed the associated 700 return periods. Each of these 700 time series has the same length as the original time series, and was built through combining randomly sampled calendar years of the precipitation and meteorological tide bivariate time series. This procedure is preferred to a classic resampling of the daily pairs, as it allows for preserving the autocorrelation of the variables. The final 95% confidence interval was then defined as the 2.5th - 97.5th percentile interval of these 700 return periods, i.e. $(T_{2.5\text{th}}, T_{97.5\text{th}})$. The associated 95% confidence interval of the variations in the return period due to natural variability was computed as the percentage difference between the observed return period and $(T_{2.5\text{th}}, T_{97.5\text{th}})$.

Symmetrized changes of the return periods for computing uncertainties in return period future changes. The uncertainty in the future changes of the return periods driven by the three individual meteorological drivers of compound flooding (precipitation, meteorological tide, and their dependence) was quantified via the intermodel spread of the *symmetrized changes of the return periods* ($\Delta T^{\text{Symmetric}}(\%)$) as explained in the next section. Here, we define the symmetrized changes of the joint return periods: for a generic return period, given $\Delta T(\%) = \Delta T(\%)(T^{\text{fut}}, T^{\text{pres}}) = 100 \cdot (T^{\text{fut}} - T^{\text{pres}}) / T^{\text{pres}}$, $\Delta T^{\text{Symmetric}}(\%)$ is defined as: $\Delta T(\%)(T^{\text{fut}}, T^{\text{pres}})$ if $\Delta T(\%)(T^{\text{fut}}, T^{\text{pres}}) > 0$, and as $-\Delta T(T^{\text{pres}}, T^{\text{fut}})$ otherwise. These symmetrized changes $\Delta T^{\text{Symmetric}}(\%)$ are preferred to simple changes $\Delta T(\%)$ as the latter tends to skew the magnitude of the uncertainty for negative return periods changes. $\Delta T(\%)$ assumes values between -100 and 0 and between 0 and $+Inf$ for negative and positive changes of the return periods, respectively. As a result, the uncertainty in $\Delta T(\%)$ would tend to appear smaller where models show a reduction of the return periods, and larger where models show

an increase of the return periods. $\Delta T^{\text{Symmetric}}(\%)$ avoids this issue as it is defined such that (i) it assumes values between $-Inf$ and 0 and between 0 and $+Inf$ for negative and positive changes of the return periods, respectively. This implies that, e.g., a doubling and halving of T^{fut} (with respect to T^{pres}) corresponds to equal but opposite values of $\Delta T^{\text{Symmetric}}(\%)$. Moreover, (ii) $\Delta T^{\text{Symmetric}}(\%)$ increases linearly with a , where $T^{\text{fut}} = a \cdot T^{\text{pres}}$ and decreases linearly with a , where $T^{\text{fut}} = 1/a \cdot T^{\text{pres}}$; this guarantees the desirable property of detecting the same return periods' intermodel spread in four situations where the six CMIP5 models project, e.g., $a = 1, 2, 3, 4, 5, 6$; $a = 1, 1/2, 1/3, 1/4, 1/5, 1/6$; $a = 1/3, 1/2, 1, 2, 3, 4$; and $a = 11, 12, 13, 14, 15, 16$.

Partitioning of return period changes and associated relative uncertainties. We assessed how the return period would change in the future when only taking into account changes (with respect to the present) of (1) the precipitation marginal distribution (i.e. the full distribution of the precipitation without reference to meteorological tide), (2) the meteorological tide marginal distribution, and (3) the dependence between the precipitation and meteorological tides^{10,14,75}. We computed the change in the return period (%) for the case (i) as $\Delta T_{\text{exp } i}^{\text{fut}}(\%) = 100 \cdot (T_{\text{exp } i}^{\text{fut}} - T^{\text{pres}})/T^{\text{pres}}$, where T^{pres} is the return period for the present period and $T_{\text{exp } i}^{\text{fut}}$ is computed as follows. Case (1): we get the empirical cumulative distribution $U_{S_{\text{pres}}}$ of the present-day sea level S_{pres} as $U_{S_{\text{pres}}} = F_{S_{\text{pres}}}(S_{\text{pres}})$ (where $F_{S_{\text{pres}}}$ is the empirical CDFs of S_{pres}). We define the empirical CDFs $F_{S_{\text{fut}}}$ of the variable S_{fut} , and define $S_1 = F_{S_{\text{fut}}}^{-1}(U_{S_{\text{pres}}})$. As a result, the variables (S_1, P_{pres}) , where P_{pres} is the present-day precipitation, have the same dependence (Spearman correlation and tail dependence¹⁴) as during the present, but the marginal distribution of S_1 is that of the future. The return period $T_{\text{exp } 1}^{\text{fut}}$ was computed based on (S_1, P_{pres}) . Case (2) was obtained as case (1), but switching precipitation and sea level variables in the procedure above. Case (3): we define $S_3 = F_{S_{\text{pres}}}^{-1}(U_{S_{\text{fut}}})$, where $U_{S_{\text{fut}}}$ is the empirical cumulative distribution of the future sea level and $F_{S_{\text{pres}}}$ is the empirical CDF of the sea level in the present climate. Similarly, we get $P_3 = F_{P_{\text{pres}}}^{-1}(U_{P_{\text{fut}}})$. As a result, the variables (S_3, P_3) have the same dependence as during the future, but the marginal distributions of the present climate¹⁴. Then, the return period $T_{\text{exp } 3}^{\text{fut}}$ was computed based on (S_3, P_3) . We observe that the total change in the return periods is not given by the sum of the changes estimated in these three cases above (the return period is not given by a linear combination of the overall marginal distribution and the dependencies).

We quantified the regional relative importance of the uncertainty in the projected changes of the three compound flooding meteorological drivers: (1) precipitation, (2) meteorological tides, and (3) their dependence (Fig. 5). We first computed (for the three cases i) the symmetrized changes of the return periods $\Delta T_{\text{exp } i}^{\text{Symmetric}}(\%)$ for the six CMIP5 models (see "Symmetrized changes" in the section above). Secondly, the contribution to the uncertainty from the change in the driver (i) (e.g., precipitation) was quantified via the intermodel spread of the $\Delta T_{\text{exp } i}^{\text{Symmetric}}(\%)$, i.e. $\sigma(\Delta T_{\text{exp } i}^{\text{Symmetric}}(\%))$. (The intermodel spread is defined as the difference between the second highest and second lowest among the six climate model projections.) Thirdly, for a given IPCC region r (Supplementary Fig. S6), we computed the regional median of $\sigma(\Delta T_{\text{exp } i}^{\text{Symmetric}}(\%))$, i.e. $\sigma_{i,r}$. Finally, the regional relative importance of each driver (i) for the uncertainty in the return period changes was quantified as $100 \cdot \sigma_{i,r} / (\sum_{i=1}^3 \sigma_{i,r})$.

Author contribution. EB conceived the study, carried out the data analysis, and drafted the manuscript. EB designed the study development with contributions from GZ and MIV. EB, MIV, and LF worked on the final manuscript with contributions from GZ. MIV, and LM performed the storm surge and wave runs. KH analysed the storm tracks. All authors discussed the results and commented on the manuscript.

References

- [1] Vousdoukas, M. I. *et al.* Global probabilistic projections of extreme sea levels show intensification of coastal flood hazard. *Nature communications* **9**, 2360 (2018).
- [2] Hinkel, J. *et al.* Coastal flood damage and adaptation costs under 21st century sea-level rise. *Proceedings of the National Academy of Sciences* **111**, 3292–3297 (2014).
- [3] Bouwer, L. M. & Jonkman, S. N. Global mortality from storm surges is decreasing. *Environmental Research Letters* **13**, 014008 (2018).
- [4] Winsemius, H. C. *et al.* Global drivers of future river flood risk. *Nature Climate Change* **6**, 381 (2016).
- [5] Pfahl, S., O’Gorman, P. & Fischer, E. Understanding the regional pattern of projected future changes in extreme precipitation. *Nature Climate Change* **7**, 423–427 (2017).
- [6] Dottori, F. *et al.* Increased human and economic losses from river flooding with anthropogenic warming. *Nature Climate Change* **8**, 781 (2018).
- [7] Jongman, B., Ward, P. J. & Aerts, J. C. Global exposure to river and coastal flooding: Long term trends and changes. *Global Environmental Change* **22**, 823–835 (2012).
- [8] Wahl, T., Jain, S., Bender, J., Meyers, S. D. & Luther, M. E. Increasing risk of compound flooding from storm surge and rainfall for major us cities. *Nature Climate Change* **5**, 1093–1097 (2015).
- [9] Paprotny, D., Vousdoukas, M. I., Morales-Nápoles, O., Jonkman, S. N. & Feyen, L. Pan-european hydrodynamic models and their ability to identify compound floods. *Natural Hazards* 1–25 (2020).
- [10] Bevacqua, E. *et al.* Higher probability of compound flooding from precipitation and storm surge in europe under anthropogenic climate change. *Science advances* **5**, eaaw5531 (2019).
- [11] Zscheischler, J. *et al.* Future climate risk from compound events. *Nature Climate Change* **8**, 469–477 (2018).
- [12] Ward, P. J. *et al.* Dependence between high sea-level and high river discharge increases flood hazard in global deltas and estuaries. *Environmental Research Letters* **13**, 084012 (2018).
- [13] Ganguli, P. & Merz, B. extreme coastal water levels exacerbate fluvial flood hazards in northwestern europe. *Scientific reports* **9**, 1–14 (2019).
- [14] Bevacqua, E., Maraun, D., Hobæk Haff, I., Widmann, M. & Vrac, M. Multivariate statistical modelling of compound events via pair-copula constructions: analysis of floods in ravenna (italy). *Hydrology and Earth System Sciences* **21**, 2701–2723 (2017).
- [15] Serafin, K. A., Ruggiero, P., Parker, K. & Hill, D. F. What’s streamflow got to do with it? a probabilistic simulation of the competing oceanographic and fluvial processes driving extreme along-river water levels. *Natural Hazards and Earth System Sciences* **19**, 1415–1431 (2019).

- [16] Kumbier, K., Carvalho, R. C., Vafeidis, A. T. & Woodroffe, C. D. Investigating compound flooding in an estuary using hydrodynamic modelling: a case study from the shoalhaven river, australia. *Natural Hazards and Earth System Sciences* **18**, 463 (2018).
- [17] van den Hurk, B., van Meijgaard, E., de Valk, P., van Heeringen, K.-J. & Gooijer, J. Analysis of a compounding surge and precipitation event in the netherlands. *Environmental Research Letters* **10**, 035001 (2015).
- [18] Couasnon, A., Sebastian, A. & Morales-Nápoles, O. A copula-based bayesian network for modeling compound flood hazard from riverine and coastal interactions at the catchment scale: An application to the houston ship channel, texas. *Water* **10**, 1190 (2018).
- [19] Ridder, N., De Vries, H. & Drijfhout, S. The role of atmospheric rivers in compound events consisting of heavy precipitation and high storm surges along the dutch coast. *Natural Hazards and Earth System Sciences* **18**, 3311–3326 (2018).
- [20] Wu, W. *et al.* Mapping dependence between extreme rainfall and storm surge. *Journal of Geophysical Research: Oceans* **123**, 2461–2474 (2018).
- [21] Zheng, F., Westra, S. & Sisson, S. A. Quantifying the dependence between extreme rainfall and storm surge in the coastal zone. *Journal of hydrology* **505**, 172–187 (2013).
- [22] Hendry, A. *et al.* Assessing the characteristics and drivers of compound flooding events around the uk coast. *Hydrology and Earth System Sciences* **23**, 3117–3139 (2019).
- [23] Paprotny, D., Vousdoukas, M. I., Morales-Nápoles, O., Jonkman, S. N. & Feyen, L. Compound flood potential in europe. *Hydrology and Earth System Sciences Discussions* 1–34 (2018).
- [24] Svensson, C. & Jones, D. A. Dependence between sea surge, river flow and precipitation in south and west britain. *Hydrology and Earth System Sciences* **8**, 973–992 (2004).
- [25] Muis, S., Verlaan, M., Winsemius, H. C., Aerts, J. C. & Ward, P. J. A global reanalysis of storm surges and extreme sea levels. *Nature communications* **7** (2016).
- [26] Couasnon, A. *et al.* Measuring compound flood potential from river discharge and storm surge extremes at the global scale. *Nat. Hazards Earth Syst. Sci.* **20**, 489–504 (2020).
- [27] Bevacqua, E., Vousdoukas, M. I., Shepherd, T. G. & Vrac, M. Brief communication: The role of using precipitation or river discharge data when assessing global coastal compound flooding. *Natural Hazards and Earth System Sciences Discussions* 1–20 (2020).
- [28] Moftakhari, H. R., Salvadori, G., AghaKouchak, A., Sanders, B. F. & Matthew, R. A. Compounding effects of sea level rise and fluvial flooding. *Proceedings of the National Academy of Sciences* **114**, 9785–9790 (2017).
- [29] Westra, S., Alexander, L. V. & Zwiers, F. W. Global increasing trends in annual maximum daily precipitation. *Journal of climate* **26**, 3904–3918 (2013).
- [30] Mentaschi, L., Vousdoukas, M. I., Voukouvalas, E., Dosio, A. & Feyen, L. Global changes of extreme coastal wave energy fluxes triggered by intensified teleconnection patterns. *Geophysical Research Letters* **44**, 2416–2426 (2017).

- [31] Morim, J. *et al.* Robustness and uncertainties in global multivariate wind-wave climate projections. *Nature Climate Change* **9**, 711–718 (2019).
- [32] Dee, D. P. *et al.* The era-interim reanalysis: Configuration and performance of the data assimilation system. *Quarterly Journal of the royal meteorological society* **137**, 553–597 (2011).
- [33] Taylor, K. E., Stouffer, R. J. & Meehl, G. A. An overview of cmip5 and the experiment design. *Bulletin of the American Meteorological Society* **93**, 485–498 (2012).
- [34] Martius, O., Pfahl, S. & Chevalier, C. A global quantification of compound precipitation and wind extremes. *Geophysical Research Letters* **43**, 7709–7717 (2016).
- [35] Salvadori, G., Durante, F. & De Michele, C. On the return period and design in a multivariate framework. *Hydrology and Earth System Sciences* **15**, 3293–3305 (2011).
- [36] Pfahl, S. & Wernli, H. Quantifying the relevance of cyclones for precipitation extremes. *Journal of Climate* **25**, 6770–6780 (2012).
- [37] Knapp, K. R., Kruk, M. C., Levinson, D. H., Diamond, H. J. & Neumann, C. J. The international best track archive for climate stewardship (ibtracs) unifying tropical cyclone data. *Bulletin of the American Meteorological Society* **91**, 363–376 (2010).
- [38] Kar-Man Chang, E. C mip5 projected change in northern hemisphere winter cyclones with associated extreme winds. *Journal of Climate* **31**, 6527–6542 (2018).
- [39] Zappa, G., Shaffrey, L. C., Hodges, K. I., Sansom, P. G. & Stephenson, D. B. A multimodel assessment of future projections of north atlantic and european extratropical cyclones in the cmip5 climate models. *Journal of Climate* **26**, 5846–5862 (2013).
- [40] Bengtsson, L., Hodges, K. I. & Roeckner, E. Storm tracks and climate change. *Journal of Climate* **19**, 3518–3543 (2006).
- [41] Zappa, G. & Shepherd, T. G. Storylines of atmospheric circulation change for european regional climate impact assessment. *Journal of Climate* **30**, 6561–6577 (2017).
- [42] Shepherd, T. G. Atmospheric circulation as a source of uncertainty in climate change projections. *Nature Geoscience* **7**, 703 (2014).
- [43] Sharma, A., Wasko, C. & Lettenmaier, D. P. If precipitation extremes are increasing, why aren't floods? *Water Resources Research* **54**, 8545–8551 (2018).
- [44] Haigh, I. D. *et al.* Spatial and temporal analysis of extreme sea level and storm surge events around the coastline of the uk. *Scientific data* **3**, 160107 (2016).
- [45] Ward, P. J. *et al.* Usefulness and limitations of global flood risk models. *Nature Climate Change* **5**, 712–715 (2015).
- [46] Patricola, C. M. & Wehner, M. F. Anthropogenic influences on major tropical cyclone events. *Nature* **563**, 339 (2018).
- [47] Olbert, A. I., Comer, J., Nash, S. & Hartnett, M. High-resolution multi-scale modelling of coastal flooding due to tides, storm surges and rivers inflows. a cork city example. *Coastal Engineering* **121**, 278–296 (2017).

- [48] Pörtner, H.-O. *et al.* IPCC special report on the ocean and cryosphere in a changing climate. *In press* (2019). URL <https://www.ipcc.ch/srocc/>.
- [49] Brown, S. *et al.* Shifting perspectives on coastal impacts and adaptation. *Nature Climate Change* **4**, 752 (2014).
- [50] Vousdoukas, M. *et al.* Economic incentives for raising coastal flood defenses in europe. *Nature communications, In press* (2020).
- [51] Zscheischler, J. *et al.* A typology of compound weather and climate events. *Nature Reviews Earth & Environment, Accepted for publication* (2020).
- [52] Vousdoukas, M. I., Mentaschi, L., Voukouvalas, E., Verlaan, M. & Feyen, L. Extreme sea levels on the rise along europe's coasts. *Earth's Future* **5**, 304–323 (2017).
- [53] Vousdoukas, M. I., Voukouvalas, E., Annunziato, A., Giardino, A. & Feyen, L. Projections of extreme storm surge levels along europe. *Climate Dynamics* **47**, 3171–3190 (2016).
- [54] Camargo, S. J. Global and regional aspects of tropical cyclone activity in the cmip5 models. *Journal of Climate* **26**, 9880–9902 (2013).
- [55] Maraun, D. *et al.* Precipitation downscaling under climate change: Recent developments to bridge the gap between dynamical models and the end user. *Reviews of Geophysics* **48** (2010).
- [56] Fernández-Montblanc, T. *et al.* Towards robust pan-european storm surge forecasting. *Ocean Modelling* **133**, 129–144 (2019).
- [57] Arns, A., Wahl, T., Dangendorf, S. & Jensen, J. The impact of sea level rise on storm surge water levels in the northern part of the german bight. *Coastal Engineering* **96**, 118–131 (2015).
- [58] Arns, A. *et al.* Sea-level rise induced amplification of coastal protection design heights. *Scientific reports* **7**, 40171 (2017).
- [59] Du, J. *et al.* Tidal response to sea-level rise in different types of estuaries: the importance of length, bathymetry, and geometry. *Geophysical Research Letters* (2018).
- [60] Howard, T., Lowe, J. & Horsburgh, K. Interpreting century-scale changes in southern north sea storm surge climate derived from coupled model simulations. *Journal of Climate* **23**, 6234–6247 (2010).
- [61] Weisse, R., von Storch, H., Niemeyer, H. D. & Knaack, H. Changing north sea storm surge climate: An increasing hazard? *Ocean & coastal management* **68**, 58–68 (2012).
- [62] Losada, I. *et al.* Long-term changes in sea-level components in latin america and the caribbean. *Global and Planetary Change* **104**, 34–50 (2013).
- [63] Chang, E. K. Projected significant increase in the number of extreme extratropical cyclones in the southern hemisphere. *Journal of Climate* **30**, 4915–4935 (2017).
- [64] Zappa, G., Hawcroft, M. K., Shaffrey, L., Black, E. & Brayshaw, D. J. Extratropical cyclones and the projected decline of winter mediterranean precipitation in the cmip5 models. *Climate Dynamics* **45**, 1727–1738 (2015).
- [65] Hodges, K. Feature tracking on the unit sphere. *Monthly Weather Review* **123**, 3458–3465 (1995).

- [66] Hodges, K. Adaptive constraints for feature tracking. *Monthly Weather Review* **127**, 1362–1373 (1999).
- [67] Hoskins, B. J. & Hodges, K. I. New perspectives on the northern hemisphere winter storm tracks. *Journal of the Atmospheric Sciences* **59**, 1041–1061 (2002).
- [68] Hodges, K. Spherical nonparametric estimators applied to the ugamp model integration for amip. *Monthly Weather Review* **124**, 2914–2932 (1996).
- [69] De Michele, C., Salvadori, G., Passoni, G. & Vezzoli, R. A multivariate model of sea storms using copulas. *Coastal Engineering* **54**, 734–751 (2007).
- [70] Serinaldi, F. Dismissing return periods! *Stochastic environmental research and risk assessment* **29**, 1179–1189 (2015).
- [71] Vandenberghe, S., Verhoest, N., Onof, C. & De Baets, B. A comparative copula-based bivariate frequency analysis of observed and simulated storm events: A case study on bartlett-lewis modeled rainfall. *Water Resources Research* **47** (2011).
- [72] Schepsmeier, U. *et al.* Vinecopula: Statistical inference of vine copulas. *R package version 2.0.5* (2016).
- [73] Heffernan, J., Stephenson, A. & Gilleland, E. Ismev: an introduction to statistical modeling of extreme values. *R package version 1.41* (2016). URL <https://CRAN.R-project.org/package=ismev>.
- [74] Bader, B. & Yan, J. eva: Extreme value analysis with goodness-of-fit testing. *R package version 0.2.4* (2016).
- [75] Manning, C. *et al.* Increased probability of compound long-duration dry and hot events in europe during summer (1950–2013). *Environmental Research Letters* **14**, 094006 (2019).